Numerical investigation of the threshold intensity dependence on gas pressure in the breakdown of xenon by different laser wavelengths

Article *in* The European Physical Journal D · July 2014

DOI: 10.1140/epjd/e2014-50111-x

CITATIONS
4

READS
150

3 authors:

Yosr E E-D Gamal
National Institute of laser Enhanced Sciences,NILES, Cairo University El Giza,Egypt
56 PUBLICATIONS **59** CITATIONS
SEE PROFILE

M. A. Mahmoud
Sohag University
8 PUBLICATIONS **26** CITATIONS
SEE PROFILE

Nagia Dawood
Taibah University
16 PUBLICATIONS **67** CITATIONS
SEE PROFILE

EPJ D
Atomic, Molecular, Optical and Plasma Physics
EPJ.org
your physics journal

Eur. Phys. J. D (2014) 68: 206 DOI: 10.1140/epjd/e2014-50111-x

Numerical investigation of the threshold intensity dependence on gas pressure in the breakdown of xenon by different laser wavelengths

Yosr E.E.-D. Gamal, Mohamed Abd El Hameid Mahmoud and Nagia D.A. Dawood

edp sciences
Società Italiana di Fisica
Springer

Eur. Phys. J. D (2014) 68: 206
DOI: 10.1140/epjd/e2014-50111-x

THE EUROPEAN PHYSICAL JOURNAL D

Regular Article

Numerical investigation of the threshold intensity dependence on gas pressure in the breakdown of xenon by different laser wavelengths

Yosr E.E.-D. Gamal[1], Mohamed Abd El Hameid Mahmoud[2,a], and Nagia D.A. Dawood[3]

[1] National Institute of Laser Enhanced Science, Cairo University, El Giza, Egypt
[2] Physics Department, Faculty of Science, Sohag University, 82524 Sohag, Egypt
[3] Physics Department, Faculty of Science, Taibah University, Al-madinah Al-monawarah, Kingdom of Saudi Arabia

Received 9 February 2014 / Received in final form 9 April 2014
Published online 29 July 2014 – © EDP Sciences, Società Italiana di Fisica, Springer-Verlag 2014

Abstract. We report a theoretical analysis of the measurements that carried out to study the breakdown of xenon gas over a wide pressure range induced by laser source operating at different wavelengths. The study provided an investigation of the effect of laser wavelength as well as gas pressure on the physical processes associated with this phenomenon. To this aim a modified electron cascade model is applied. The model based on the numerical solution of the time dependent Boltzmann equation for the electron energy distribution function (EEDF) simultaneously with a set of rate equations which describe the rate of change of the formed excited states population. Comparison between the calculated and measured threshold intensities for the experimentally tested laser wavelengths and gas pressure range is obtained. Furthermore computations of the EEDF and its parameters showed the actual correlation between the gain and loss processes which determine the threshold breakdown intensity of xenon and the two experimentally tested parameters; laser wavelength and gas pressure.

1 Introduction

During the last few decades, the phenomenon of optical breakdown of gases has been the subject of many investigations [1–11] due to its important applications in different scientific and science life fields. Practically this phenomenon was found to depend on both laser characteristics and nature of gas.

Therefore the application of this phenomenon in the different fields requires an accurate study of the laser characteristics applied in such field. This is the role played by physicists to determine the laser characteristics such as laser intensity, pulse duration and the associated wavelength.

Many experimental measurements are carried out together with theoretical calculations using numerical models to investigate this phenomenon [12–24]. These studies revealed, with great success many of the physical concepts which are associated with the interaction of laser radiation, having infrared and visible spectrum [19]. Whereas when lasers with short wavelengths are used, the investigation of this phenomenon still represents an open question [18].

Accordingly, in the present work a theoretical investigation of the breakdown phenomenon of xenon gas using laser source operating at different wavelengths is presented. This study is particularly devoted to investigate the effect of laser wavelength, as well as gas pressure on the physical processes associated with this phenomenon. This gas is deliberately chosen due to its importance as a buffer gas in the generation of the X-ray laser from solid targets, in addition to its use as interacting gas for excimer laser operation. The study based on a modified electron cascade model [2] given by Evans and Gamal [3].

In contrast to the previously developed electron cascade models which are performed to study the gas breakdown phenomenon based on a classical or a quantum-mechanical treatment of the time independent Boltzmann equation, disregarding the effect of laser pulse shape [12,13], in the present model the electron energy distribution function is taken to vary with time and thus more realistically represents the conditions found in practice. Moreover, an energy-diffusion term is introduced in the applied Boltzmann equation. This term was obtained automatically by Zel'dovich and Raizer [6], from calculations of the electron energy gain based on the quantum-mechanical treatment of the Boltzmann equation. The importance of this term has been stressed by these authors, using an argument similar to the following. Consider a simple gas which has ionization potential E_i and an excitation potential E_{ex} ($<E_i$). When electrons gain energy steadily at the mean rate, and when the energy gain per collision $\varepsilon_0 < E_i - E_{ex}$, then they cannot reach the energy E_i without spending some time in the interval between

[a] e-mail: hameideg@yahoo.com

E_{ex} and E_i. In this interval, the electrons are able to lose energy by excitation, and this clearly reduces the number of electrons which can reach the energy E_i. For atomic gases, omission of the energy-diffusion term can produce a large error, for example in the calculated threshold intensity for breakdown. On the other hand, in this model excited atoms, however, are allowed to be ionized by electrons with energy $\varepsilon < E_i - E_{ex}$ eV. The presence of a large number of excited atoms therefore lowers the average ionization potential of the gas and leads to an increased rate of ionization. The process of collisional ionization of excited atoms is referred to as "two-step ionization"; it becomes appreciable only towards the later stages of plasma development when a large fraction of the gas atoms has become excited, and is a second-order process-that is, its rate is approximately proportional to the square of the ionization density.

It is possible, also, for excited atoms to be more readily photo-ionized by the laser light. The rate for this process is proportional to (the instantaneous laser intensity) q, where q is the number of absorbed photons an atom to be ionized. Both processes may make a relatively small difference to the breakdown threshold intensity, since even if the respective cross-sections were infinite, the net effect would be to lower only the ionization potential from E_i to E_{ex}, with a roughly proportional change in the threshold intensity.

Consequently, the model solves numerically the time dependent Boltzmann equation for the electron energy distribution function (EEDF) simultaneously with a set of rate equations, which describe the change of the formed excited states population. Calculations are carried out to investigate the experimental measurements that given by Davis et al. [1] to study the breakdown of xenon induced by a Nd:YAG laser source operated at its first four harmonics of wavelengths 1064, 532, 355 and 266 nm corresponding to pulse duration 8.5, 7.5, 6.5 and 5.5 ns, respectively with a raw beam diameter of 0.6 cm. The spot sizes at the focal plan were 5.7×10^{-5} cm^2 for 1064, 532 and 355 nm and 6.4×10^{-5} cm^2 for 266 nm. These correspond to beam diameters 8.52×10^{-3} cm and 9.02×10^{-3} cm, respectively. The threshold fluence energy for the four laser wavelengths is obtained at the atmospheric pressure to be 221, 63, 128 and 28 J/cm^2, respectively. While, the measured threshold intensity over the examined pressure range (25 to 760 torr) is found to vary from $\sim 5.2 \times 10^9$ to 3.2×10^{11} W/cm^2.

The results of computations provided a relation between the threshold intensity as a function of gas pressure for each laser wavelength. In addition computations of the electron energy distribution function and its parameters at the atmospheric pressure clarified the correlation between the physical process corresponding to xenon breakdown threshold intensity and laser wavelength.

2 Theoretical formulation

The theoretical approach used to describe the electron cascade model is given in details in reference [2,3]. This model takes into account the electron energy gain through the absorption of the laser energy by inverse bremsstrahlung process followed by collisional ionization processes which lead eventually to the gas breakdown. In addition to this process, electrons can also be generated through multiphoton absorption process of the ground and the formed excited atoms.

The model is applied to xenon atom, which is assumed to have three levels namely: ground state, one excited state and an ionized state. Accordingly, the following collisional and radiative processes are considered: (i) electron inverse-Bremsstrahlung absorption; (ii) electron impact excitation of by electrons of energy $\varepsilon > 8.32$ eV; (iii) electron impact ionization of ground state atoms by electrons having energies $\varepsilon > 12.13$ eV; (iv) collisional ionization of the excited state by electrons having energies $\varepsilon >$ (12.13–8.32) eV; (v) photo-ionization of the ground and excited atoms (vi) electron diffusion losses and (vii) electron recombination.

In this model the inclusion of the two-step collisional ionization process is found to have increasing importance with the increase of the gas pressure, due to the increase of excitation to ionization events ratio [3]. Also the role of multiphoton ionization process is unlikely to occur in unexcited xenon atoms in comparable to the case of excited xenon at the IR and visible laser wavelengths. This in turn affects to some extent the determination of the breakdown threshold intensity values.

Consequently the equation which represents the energy gained by free electrons from the laser field is written as:

$$\frac{\partial f(\varepsilon,t)}{\partial t} = \frac{2\varepsilon}{3m\nu_m(\varepsilon)}\nabla^2 f + \frac{1}{3}\varepsilon_0\nu_m(\varepsilon)\frac{\partial f}{\partial \varepsilon} + \frac{2}{3}\varepsilon_0\nu_m(\varepsilon)\frac{\partial^2 f}{\partial \varepsilon^2} + Inelastic\ \ collision\ \ terms, \quad (1)$$

where $f(\varepsilon,t)d\varepsilon$ denotes the number density of electrons with energy between ε and $\varepsilon + d\varepsilon$, $\varepsilon_0 = e^2E^2/2m\omega^2$ is the average oscillatory energy of an electron in the laser field with electric field amplitude E and angular frequency ω, $\nu_m(\varepsilon)$ is the momentum transfer collision frequency between electron and gas atom. In this equation, the first term on the right-hand side represents the rate of electrons loss from the radiated volume due to diffusion. This term is responsible for the focal volume dependence on the breakdown threshold, and is influenced by the frequency of the incident radiation [25]. Here, we shall rewrite this term by setting $\nabla^2 f = -\Lambda^{-2} f$, where Λ is the characteristic diffusion length [7]. This length characterizes the distance over which a particle should diffuse in order to be lost from the plasma. Following standard optical focal theory, the minimum focal volume is assumed to be cylindrical [26] of radius $r_0 = f_l\ (\alpha/2)$ and axial length $l_0 = (2\sqrt{2}-1)(\alpha/d)f_l^2$, where f_l is the focal length of the lens, d is the diameter of the unfocused laser beam and α the corresponding beam divergence [7]. The second term represents the electron energy gain from the laser field. The third term is referred to electron energy diffusion along the energy axis [3]. This energy-diffusion term, has been obtained from classical arguments based on expressions for the mean energy gain per collision for

various types of interactions given by Pert [27]. This term is analogous to the term involving energy diffusion appeared in the energy gain equation derived by Zel'dovich and Raizer [6] as a consequence of using a quantum-mechanical treatment. This energy- diffusion term allows the possibility of an electron gaining appreciably more (or, of course, less) than the mean energy in a collision, and therefore of moving directly from an energy < the excitation threshold (E_{ex}) to an energy > the ionization threshold (E_i). Ionization then becomes a more likely event. For atomic gases, omission of this term may produce a large error in the calculation of the threshold intensity for breakdown. The inelastic collision terms include generation of electrons with energy ε through ionization of ground and excited atoms as well as atomic excitation by electron impact. It also comprises electron losses through recombination processes.

Equation (1) is solved numerically using a step-by-step integration. The step-length in energy $\Delta\varepsilon$ was chosen so that the complete energy distribution could be represented by about 25 equally spaced points. This covers and exceeds the first ionization energy threshold of xenon at 12.13 eV. The derivatives $\partial f/\partial\varepsilon$ and $\partial^2 f/\partial\varepsilon^2$ were evaluated using the finite difference technique. The ionization and excitation terms as well as the loss processes terms could have been included as difference terms in equation (1), but there are good reasons for treating them separately [3]. Each ionization or excitation of an atom leads to reduction of the neutral atoms present in the focal volume; this case is also considered into the model.

The breakdown criteria used in this analysis is taken as attainment of degree of fractional ionization $\delta \approx 0.1\%$ of the neutral gas atoms present in the focal volume. The temporal variation of the laser intensity in the focal volume is assumed to have a Gaussian distribution of the form:

$$I(t) = I(0)A\left(e^{\frac{-(t-\tau)^2}{4\tau^2}} - B\right), \tag{2}$$

where the constants $A = 4.5208$ and $B = 0.7788$, $I(0)$ is the laser peak intensity and 2τ is the laser pulse width (FWHM).

According to the assumed geometric optics consideration, the value of the cylindrical focal volume is calculated to be of the order of 10^{-8} cm^3. To speed up the calculations two time steps are used to solve equation (1); short time step for calculating the elastic collisional terms (electron energy gain terms) and long time step which used for the inelastic collisional processes. For the continuity of the electron energy distribution function, the initial electron density before firing the laser pulse is assumed to have Gaussian distribution with its peak at 4 eV.

2.1 Cross-sections and rate coefficients

Cross sections and rate coefficients of xenon gas corresponding to the kinetic reactions considered in this analysis are taken from experimental data available in literature as follows:

2.1.1 Momentum transfer cross-section

In the present calculations, the exact correlation between the electron energy and the cross-section is considered. This was obtained by applying a least square fit technique to the experimental data given by Hayashi [28] such as:

$$\sigma_m(\varepsilon) = \Big(-0.44225 + 0.86703 \times \varepsilon - 0.13383 \times \varepsilon^2 + 0.00874 \times \varepsilon^3 - 2.60921 \times 10^{-4} \times \varepsilon^4 + 2.91916 \times 10^{-6} \times \varepsilon^5 \Big) \times 10^{-15} \text{ cm}^2. \tag{3}$$

2.1.2 Collisional excitation cross section

The cross section of collisional excitation of the exited state is taken from data given by Puech and Mizzi [29] to be:

$$\sigma_x(\varepsilon) = -12.60533 + 3.65404\varepsilon - 0.36088\varepsilon^2 + 0.01654\varepsilon^3 - 3.60309\varepsilon^4 \times 10^{-4} + 3.01159\varepsilon^5 \times 10^{-6} \text{ cm}^2. \tag{4}$$

2.1.3 Cross section of collisional ionization

We presumed for the cross section of collisional ionization of ground state xenon atom the data given by Puech and Mizzi [29]:

$$\sigma_i(\varepsilon) = -6.980 \times 10^{-16} + 7.490\varepsilon \times 10^{-17} - 1.784\varepsilon^2 \times 10^{-18} + 1.544\varepsilon^3 \times 10^{-20} \text{ cm}^2. \tag{5}$$

2.1.4 Two-step collisional ionization cross section

Due to the lack of experimental measurements on this cross-section, we adopted the assumption given by Evans and Gamal (1980) [3] that the cross section of collisional ionization of the excited state has the same functional form as that considered for the ground state atoms multiplied by 10^2 as follows:

$$\sigma_{ex}(\varepsilon) = \Big(-6.980 \times 10^{-16} + 7.490\varepsilon \times 10^{-17} - 1.784\varepsilon^2 \times 10^{-18} + 1.544\varepsilon^3 \times 10^{-20} \Big) \times 100 \text{ cm}^2. \tag{6}$$

2.1.5 Multiphoton ionization rate coefficient

The rate coefficient of multiphoton ionization of ground and excited atoms is calculated using a relation given by Grey-Morgan [8] such as:

$$A = \frac{\sigma^q}{\nu^{2q-1}(q-1)!h^q}, \tag{7}$$

Table 1. Calculated photoionization coefficient for ionizing the excited xenon atoms at the different values of the laser wavelength, together with the number of absorbed photons (q) as well as their corresponding energy E_{ph}, the amount of energy required for ionization E_{ix}, and the excess energy(ΔE).

Wavelength (nm)	The photon energy (eV)	$E_{ix} = (E_i - E_x)$ (eV)	Number of absorbed photons (q)	$E_{ph} = qh\nu$ (eV)	$\Delta E = E_{ph} - E_{ix}$ (eV)	Photoionization Coefficient $(\text{cm}^2\ \text{w}^{-1})^q\ \text{s}^{-1}$
1064	1.165	3.810	4	4.660	0.850	6.133×10^{-50}
532	2.331	3.810	2	4.662	0.852	1.273×10^{-18}
355	3.493	3.810	2	6.986	3.176	3.782×10^{-19}
266	4.661	3.810	1	4.661	0.851	1.339×10^{-2}
		12.130	3	13.983	1.853	9.452×10^{-37}

where, σ is the photo-absorption cross-section ($\sim 10^{-18}$ cm^2) [30], ν is the laser frequency, h is Planck's constant and q is the number of photons absorbed by an atom to be ionized. Using this formula Table 1 shows the calculated rate coefficients expressed in $(\text{cm}^2\ \text{w}^{-1})^q\ \text{s}^{-1}$ for ionizing the excited state (8.32 eV) for the wavelengths 1064, 532 and 355 nm, where q is the number of absorbed photons. While for the shortest wavelength (266 nm) this coefficient is calculated for both excited and ground state atoms. In addition the photon energy, the absorbed photons energy, the amount of energy required for ionizing the atoms ($E_{ix} = E_i - E_{ex}$ eV), as well as the excess energy that carried by the emitted electron ($\Delta E = E_{ph} - E_{xi}$ eV) are also shown in this table.

2.1.6 Electron diffusion rate

Diffusion losses can take place during the laser pulse with high probability over the low gas pressure regime; the rate of electron energy loss by electrons having an energy ε due to diffusion is given by [7]:

$$A_D(\varepsilon) = \frac{2\varepsilon}{3m\nu_m}\Lambda^{-2}, \tag{8}$$

where $\Lambda = d/2.405$, is the diffusion length of electrons in a cylindrical focal volume of radius much less than its axis i.e $r_0 \ll l_0$.

2.1.7 Electron-ion recombination rate coefficients

Electron-ion recombination considers both radiative recombination and three-body recombination processes. The rate coefficients of these processes are estimated from relations given by Wely and Rosen [16]. The radiative recombination rate coefficient R_{rad} is given by:

$$R_{\text{rad}} = \frac{0.09}{\varepsilon^{0.6}}. \tag{9}$$

The three body recombination rate coefficient R_{tb} is represented by:

$$R_{tb} = \frac{4.6 \times 10^{-14}}{V^2 \times \varepsilon^{\frac{9}{2}}}. \tag{10}$$

In these equations V is the focal volume and ε is the electron energy expressed in eV.

3 Results and discussion

Calculations are carried out to investigate the breakdown of xenon induced by a Nd:YAG laser source which operates at its first four harmonics with wavelengths 1064, 532, 355 and 266 nm and pulse duration 8.5, 7.5, 6.5 and 5.5 ns, respectively. The measured threshold irradiance over pressure range 25 to 760 torr is found to vary between 5.2×10^9 to 3.2×10^{11} W/cm^2. These experimental conditions correspond to [1]. The computations provided the threshold intensity as a function of gas pressure. Comparison between the calculated thresholds and the experimentally measured ones is shown in Figure 1 for the four laser wavelengths (a) 1064 nm, (b) 532 nm, (c) 355 nm and (d) 266 nm. From this figure it is shown that the calculated threshold intensities as a function of gas pressure are in reasonable agreement with the experimentally measured ones for all laser wavelengths. Inspection of these curves revealed that at a selected value of gas pressure the threshold irradiance varies unsystematically with the laser wavelength as shown in Figure 2. This figure showed also that the lowest value of the threshold intensity is observed at the wavelength 266 nm, while the highest one corresponds to the wavelength 355 nm. This result agrees with the experiment which assures the validity of the model.

The unsystematic behavior of the threshold intensity with the laser wavelength is mainly attributed to the role played by the physical processes which control the breakdown phenomenon. This was identified during the calculation of the threshold intensity as a function of gas pressure at each laser wavelength. For example for the laser wavelength 532 nm (curve b) the agreement between the calculated thresholds and the measured ones is obtained in the absence of loss processes. This in turn illustrates their low values. While for the longest wavelength (curve a) the agreement is satisfied in the presence of the combined effect of the two loss processes. At wavelength 355 nm (curve c) calculations revealed that the threshold intensity is mainly controlled by diffusion losses. For the shortest laser wavelength curve (d) ($\lambda = 266$ nm) different behavior is shown, where the calculations showed a noticeable competition between the electron loss and gain processes over the whole tested gas pressure range.

This result encouraged us to study the physical processes responsible for the breakdown phenomenon for each

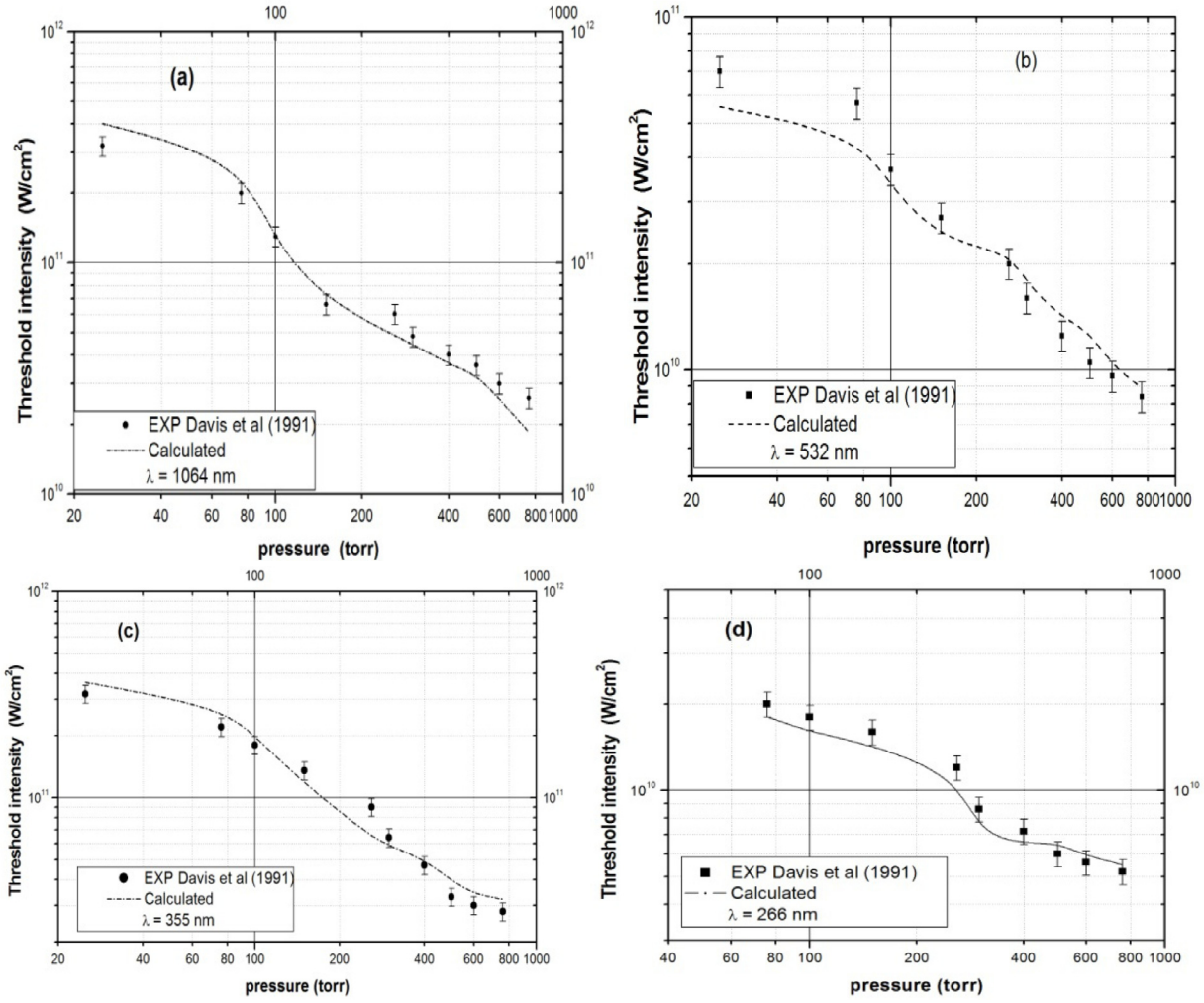

Fig. 1. Comparison between the calculated thresholds and the experimentally measured values for the four laser wavelengths (a) 1064 nm, (b) 532 nm, (c) 355 nm and (d) 266 nm.

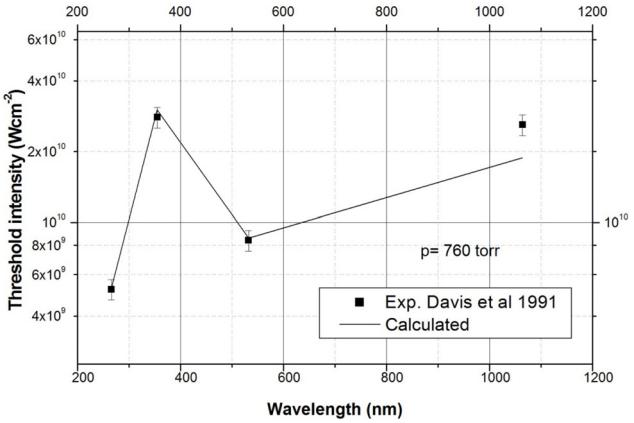

Fig. 2. Variation of the threshold intensity as a function of the laser wavelength at the atmospheric gas pressure.

laser wavelength. In doing so Figure 3 represents the electron energy distribution function (EEDF) calculated for the atmospheric pressure at the end of the laser pulse for the laser the wavelengths 1064 nm (curve a), 532 nm (curve b), 355 nm (curve c) and 266 nm (curve d). From this figure it is shown that at the very low energy regime (>0.0 eV and ⩽1.0 eV) the values of the EEDF corresponding to curves (a) and (b) ($\lambda = 1064$ nm and 532 nm) lie above those represented by curves (c) and (d) ($\lambda =$ 355 nm and 266 nm). This result could interpret significantly the effect of electron losses due to diffusion out of the focal volume at these wavelengths. Beyond this energy it is noticed that the lowest values of the EEDF correspond to the wavelength 532 nm (curve b), while the highest ones match the wavelength 266 nm (curve d). This behavior points out the role played by the photoionization process associated with the shortest wavelength. On the energy range 1.0–8.0 eV (below the threshold excitation energy) the EEDF's displayed almost leveling off behavior. Beyond this energy a sudden drop of the EEDF's is perceived as shown by curves (a)–(d). This drop reflects the loss of electrons energy through inelastic collisional excitation. The tail of the EEDF's is directed towards the energy region which lies below the ionization limits (12.13 eV).

To get a deeper insight into the exact contribution of the physical processes to the electrons density growth

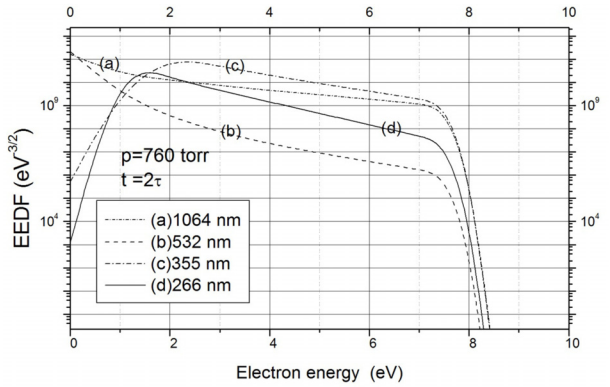

Fig. 3. The calculated EEDF at atmospheric pressure at the end of the laser pulse for the four laser wavelengths.

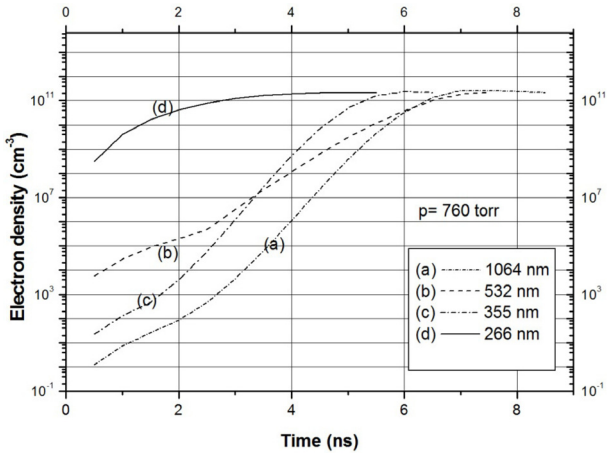

Fig. 4. Temporal evolution of the electron density during the laser pulse calculated at the atmospheric pressure for each laser wavelength curve (a) 1064 nm, curve (b) 532 nm, curve (c) 355 nm and curve (d) 266 nm.

rate, calculations are carried out to obtain the time evolution of the electron density during the laser pulse at the atmospheric pressure. These are shown in Figure 4 for the wavelengths; 1064 nm curve (a), 532 nm curve (b), 355 nm curve (c) and 266 nm curve (d). The result shown in this figure illustrates that the increase of the electrons density is controlled mainly by photon ionization of the formed excited state for the curves (b)–(d). This is indicated from the high values of the electron density observed during the early stages of the laser pulse which is clearer for the shorter wavelength (curve d). This could be attributed to the effective ionization rate of ground and excited atoms through photo-ionization mechanism. The decrease of the electron density during this period shown for curve (c) clarifies the role played by diffusion losses. On the other hand the slow growth rate of electrons shown by curves (a)–(c) during the first half of the laser pulse confirms the role played by collisional processes in populating the excited state. The saturation behavior shown on the second half of the laser pulse for curves (a)–(d) points out the competition between rate of free electrons generation through electron impact ionization and photoionization processes and the rate of electrons loss by diffusion and/or recombination. In this figure it is noticed that the electron density for the four curves terminates with the same value at the end of the laser pulse. This is referred to the constant gas pressure value (and hence the breakdown criterion) considered in this analysis at which the calculations are performed.

To confirm this result the number of ionizations per electron per ns, $(1/n)\ dn/dt$), is calculated for different time intervals during the laser pulse at the atmospheric pressure and shown in Figure 5 curves (a)–(d) for the considered laser wavelengths. From this figure it is shown that the calculated values corresponding to the laser wavelengths 1064 nm and 355 nm (curves a, c) follow almost the laser pulse shape. For the shortest wavelength (curve d) however, different behavior is observed where the calculations showed noticeable increase in the number of ionizations at the early stages of the laser pulse followed by a sharp decrease which is continued gradually up to its the end. This behavior explains the immediate growth rate of the electron density through photoionization process once firing on the laser source. This high electron density is overcome by the high loss rate through diffusion and recombination processes. This action is more pronounced during the descending part of the laser pulse leading to the leveling off behavior illustrated by curve (d) in this figure. For the wavelength 532 nm (curve b) the calculated values are considerably lower and showed some oscillations. This behavior could be attributed to the low threshold intensity associated with this wavelength as well as the absence of electron losses. This dissimilar behavior of the number of ionizations per electron per ns obtained for the four laser wavelength gives an evidence for the different contribution of the physical mechanisms to the breakdown phenomenon.

To approve this result calculations are performed to obtain the time variation of the electron mean energy at the atmospheric gas pressure, as a function of the laser wavelength as shown by curves (a)–(d) in Figure 6. This relation showed an unpredictable behavior for the variation of the electron mean energy with time for the different laser wavelengths. It is noticed from this figure that the lowest values of the electron mean energy correspond to the wavelength 532 nm (curve b), while the highest ones correspond to the 355 nm (curve c). These results are in agreement with the behavior shown for the number of ionization per electron per ns for the same wavelengths. Despite the high value shown by curve (a) during the early stages of the laser pulse the electron mean energy for the wavelength 1064 nm is almost time independent. It is also noticed here that curves (a)–(c) undergo a noticeable increase during the second half of the laser pulse. This could be attributed to the low growth rate of the electron energy during this period so electrons can only accumulate an amount of energy which is not high enough to undergo inelastic collisions.

For completeness, Figures 7a–7d shows the contour representation of the time evolution of the electron density corresponding to explicit electron energy range (EEDF)

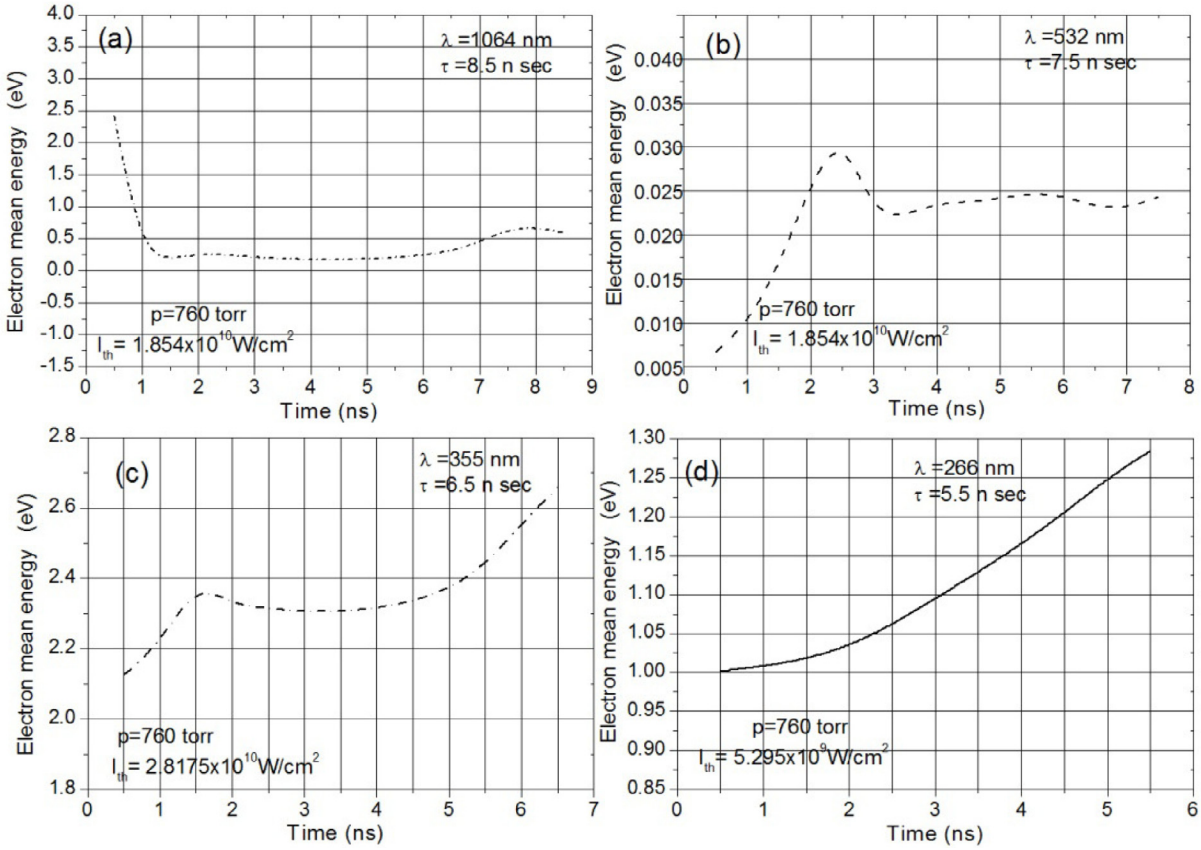

Fig. 5. The number of ionizations per electron per ns calculated at different time intervals during the laser pulse at atmospheric pressure for the different laser wavelengths.

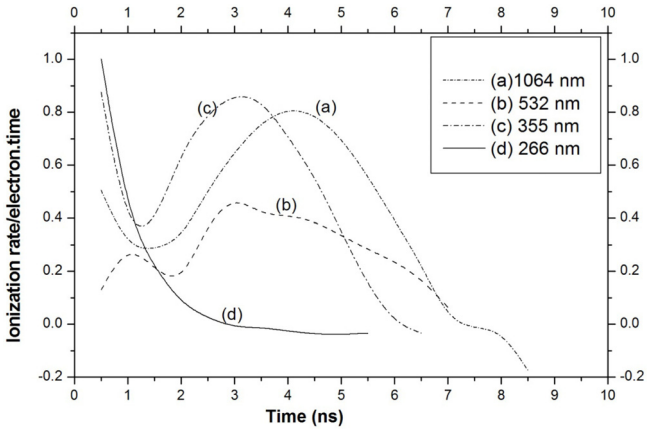

Fig. 6. Variation of the electron mean energy as a function of time at the atmospheric pressure for the four laser wavelengths.

plotted for the four wavelengths at atmospheric pressure. This figure showed the time at which breakdown occurs as well as the energy region of the highest electrons density corresponding to each laser wavelength. It is clear from this figure that at the short laser wavelength (Fig. 7d) the breakdown region extends over a longer period during the laser pulse with electrons possess low energy value (∼1.0 eV). This result assures that breakdown occurs mainly through photoionization processes which are normally effective around the peakof the pulse. For $\lambda = 355$ nm (Fig. 7c) diffusion losses are acting more effectively which results in some delay for the breakdown process to a time interval lies near the end of the pulse. It is also noticed here that the highest density of electrons possess energy of the order of 2.0 eV. This delay of the plasma formation gives an evidence for the high loss rate of the energetic electrons out of the focal volume through diffusion. For the longer wavelengths (Figs. 7a and 7b) the breakdown occurs near the end of the pulse with electrons having low energy values of (<1.0 eV). This indicates that ionization proceeds mainly through collisional processes. This study showed also the important role played by the loss processes in controlling the breakdown threshold intensity as a function of the laser wavelength.

4 Conclusions

The investigation given in this study provided a plausible interpretation of the physical processes involved during the breakdown of xenon at a pressure range 25–760 torr by the first four harmonics of a Nd:YAG laser radiation at wavelengths 1064, 532, 355 and 266 nm.

– The predicted threshold intensities showed reasonable agreement with the experimentally measured ones

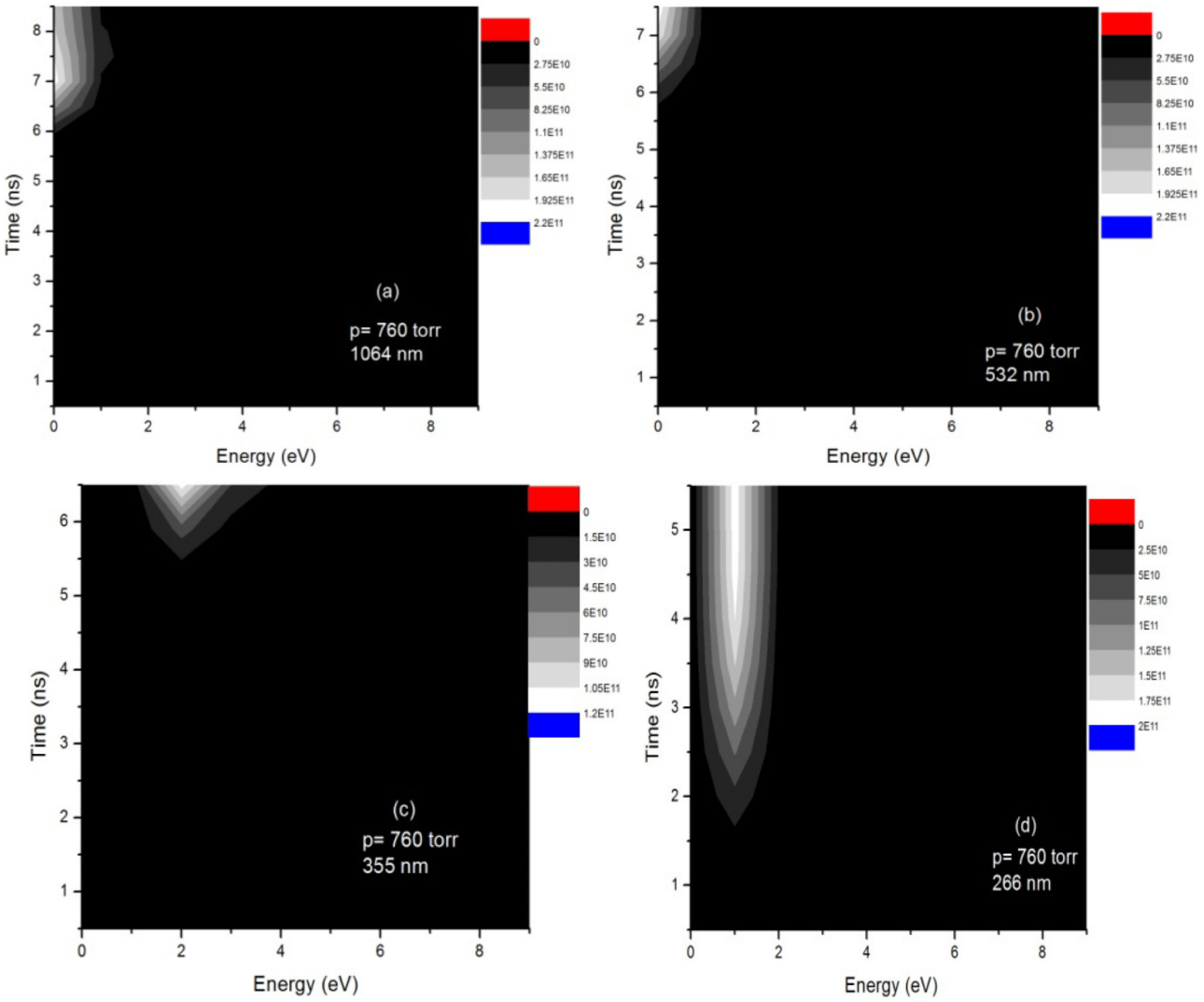

Fig. 7. Contour representation of the time evolution of the EEDF plotted for the four wavelengths at atmospheric pressure.

given by Davis et al. [1] for each laser wavelength over the tested gas pressure range.

- Plotting the threshold intensity as a function of the laser wavelength at the atmospheric pressure showed high threshold intensities for the wavelengths 355 and 1064 nm. This was attributed to the high competition between electron gain and loss processes, since the residual energy that carried out by the emitted photoelectrons matches to some extend the threshold energy for diffusion losses.
- Moreover, calculations of the temporal evolution of; the EEDF, electrons growth rate, number of ionization per electron per ns, as well as the electron mean energy elucidated the correlation between the laser wavelength, gas pressure and the physical mechanisms responsible determining the threshold intensity for breakdown.
- The contour representation of the time evolution of the EEDF plotted at atmospheric pressure showed the time at which breakdown occurs as well as the size of the highest electron region and its corresponding energies for each laser wavelength.

References

1. J.P. Davis, A.L. Smith, C. Giranda, M. Squicciarini, Appl. Opt. **30**, 4358 (1991)
2. Y.E.E.-D. Gamal, I.M. Azzouz, J. Phys. D **34**, 3234 (2001)
3. J.C. Evans, Y.E.E.-D. Gamal, J. Phys. D **13**, 1447 (1980)
4. R.G. Meyer, A.F. Haught, Phys. Rev. Lett. **11**, 401 (1963)
5. N. Isenor, Can. J. Phys. **42**, 1413 (1964)
6. Y. Zel'dovich, Y. Raizer, Sov. Phys. J. Exp. Theor. Phys. **20**, 772 (1965)
7. N. Kroll, K.M. Watson, Phys. Rev. A **5**, 1883 (1972)
8. C.G. Morgan, Rep. Prog. Phys. **38**, 621 (1975)
9. Y. Gontier, M. Trahin, Phys. Rev. A **19**, 264 (1979)
10. G. Wely, D. Rosen, J. Wilson, W. Seka, Phys. Rev. A **26**, 1164 (1982)
11. I.C.E. Turcu, M.C. Gower, P. Huntington, Opt. Commun. **134**, 66 (1997)

12. M. Louis-Jacquet, A. Decoster, J. Phys. B **19**, 197 (1977)
13. P.E. Nielson, G.H. Canavan, S.D. Rockwood, Proc. IEEE **59**, 709 (1971)
14. E.J. Button, A. Guenther, Appl. Phys. **47**, 522 (1976)
15. L. Friedland, Phys. Rev. A **12**, 202 (1975)
16. G.M. Wely, D. Rosen, Phys. Rev. A **31**, 2300 (1985)
17. D. Rosen, G. Wely, J. Phys. D **20**, 1264 (1987)
18. T.X. Phuoc, Opt. Commun. **175**, 419 (2000)
19. Y.E.E.-D. Gamal, M.M. Omar, Radiat. Phys. Chem. **62**, 361 (2001)
20. J.J. Camacho, J.M. Poyato, L. Díaz, M. Santos, J. Phys. B **40**, 4573 (2007)
21. J.J. Camacho, M. Santos, L. Díaz, J.M. Poyato, J. Phys. D **41**, 215206 (2008)
22. Y.E.E.-D. Gamal, M.M. Omar, Egypt. J. Phys. **41**, 1 (2011)
23. Y.E.E.-D. Gamal, K.A. El Sayed, M.A. Mahmoud, Opt. Laser Technol. **44**, 2154 (2012)
24. A. Sircar, R.K. Dwivedi, R.K. Thareja, Appl. Phys. B **63**, 623 (1996)
25. A.J. Alcock, K. Kato, M.C. Richardson, Opt. Commun. **6**, 342 (1972)
26. A.D. MacDonald, *Microwave Breakdown in Gases* (Wiley, New York, 1966)
27. G.J. Pert, J. Phys. A **5**, 506 (1972)
28. M. Hayashi, Nagoya University Report No. IPPJ-AM-19, 1981
29. V. Puech, S. Mizzi, J. Phys. D **24**, 1974 (1991)
30. I.I. Sobel'man, *Vvedenie v teoriyu atomnykh spektrov (Introduction to the Theory of Atomic Spectra)* (Fizmatgiz, 1963)